Integration of pumped thermal energy storage systems based on Brayton cycle with CSP plants

Mario Petrollese[a], Mario Cascetta[b], Daniele Cocco[c], Vittorio Tola[d] and Giorgio Cau[e]

[a] University of Cagliari, Cagliari, Italy, petrollese@unica.it, CA
[b] University of Cagliari, Cagliari, Italy, mcascetta@unica.it
[c] University of Cagliari, Cagliari, Italy, daniele.cocco@unica.it
[d] University of Cagliari, Cagliari, Italy, vittorio.tola@dimcm.unica.it
[e] University of Cagliari, Cagliari, Italy, gcau@unica.it

Abstract:

In this paper, the integration of Brayton cycle PTES systems with Concentrating solar power (CSP) plants is proposed and investigated. Specific mathematical models were developed to simulate the PTES and CSP sections as well as to calculate the thermal profiles of the different TES storage tanks during the charging and discharging phases. As case study, an integrated PTES-CSP system using argon as working fluid and characterized by a nominal power of 5 MW and a nominal storage capacity of 4 equivalent hours of operation is considered. The influence of the main design parameters on two performance indexes, namely, the charge-to-discharge efficiencies of the sole PTES section and the integrated PTES-CSP plant, have been investigated. The results demonstrate that the use of high values of pressure ratio is beneficial for the charge-to-discharge efficiency of the integrated plant, even if too high operating pressures could be detrimental for the design of the solar receiver and the high temperature storage tank. The low temperature TES is a critical component due to its cryogenic operating conditions, but an increase in the minimum temperature should be achieved by increasing the inlet temperature of the LP compressor. A sensitivity analysis on the compressor and turbine efficiencies, maximum and minimum temperatures, circuit pressure drop and working fluid has been carried out. Finally, a feasible design of the PTES-CSP system with a PTES roundtrip efficiency of nearly 52% and a charge-to-discharge efficiency of the integrated PTES-CSP plant of about 36% was proposed.

Keywords:
Energy Storage; Concentrating Solar Power; Pumped Thermal Energy Storage; Packed bed Thermal Energy Storage.

1. Introduction

Pumped Thermal Energy Storage (PTES) is a promising electrical energy storage technology characterized by high energy density, high roundtrip efficiency and no requirements of special sites for its installation [1]. PTES systems are constituted by a power block that can operate both as heat pump and heat engine and a Thermal Energy Storage (TES) system constituted by a low temperature (LT) reservoir and a high temperature (HT) reservoir. During the charging process, electricity is used to pump heat from the LT reservoir to the HT reservoir through a reverse power cycle. During the discharging process, the stored thermal energy is converted into electricity through a power cycle. In recent years, various PTES systems have been proposed based on different cycles, such as Rankine and Brayton cycles [2]. Among them, the research on PTES based on Brayton cycle is currently the most advanced with studies on various plant configurations, in-depth analyses on their thermodynamic aspects and on performance evaluation under different operating conditions [3]. In this regard, the effect on main performance indexes of the design solutions as maximum and minimum cycle temperatures and pressure ratios was investigated by Guo et al. [4], finding the optimal configuration of a Brayton-based PTES system. However, as highlighted by McTigue et al. [5], the achieved performance in terms of roundtrip efficiency are strongly sensitive to the loss factors that occur in compression and expansion processes. An alternative PTES configuration was proposed by

Benato [6], in which an electrical heater is included after the compressor to convert electrical energy into thermal energy, aiming to make the maximum cycle temperature independent from the compressor pressure ratio. Although the presence of the electrical heater reduces the roundtrip efficiency, the author demonstrated that a decrease in heat exchange areas and compressor size and, thus, in PTES specific costs is expected. The thermodynamics and heat transfer process affecting the PTES performance were also investigated by Wang et al. [7], highlighting the importance of the main design parameters of the TES systems, as particle size, aspect ratio etc., to achieve the maximum roundtrip efficiency and a suitable discharging power stability. In all the previous papers, the TES section is based on packed bed sensible heat storage systems, while the most common working fluid is argon. However, other working fluids, such as air, carbon dioxide, helium, etc. have been studied [8]. As stated by Dumont et al. [9], roundtrip efficiencies of about 60 – 70% are often claimed in the literature, but these values are achieved with very high compressor/turbine polytropic efficiencies (over 90%). Since the latter have a considerable impact on the efficiency of the Brayton-PTES system, a strong reduction in roundtrip efficiency would be expected if slightly lower polytropic efficiencies were assumed. For this reason, innovative solutions should be investigated for making such storage systems competitive with the common storage technologies (such as pumped hydro and compressed air energy storage systems).

In this paper, the integration of Brayton cycle PTES systems with Concentrating Solar Power (CSP) plants is proposed and investigated. CSP is an effective technology to convert solar energy into electricity, but the intermittent nature of solar radiation limits the capacity factors achievable by these systems. The integration of CSP plants with PTES systems is a possible solution to overcome this limitation, increasing the plant dispatchability and the capacity factor. Moreover, the possible sharing of some components between the two sections (such as the power generation section and the TES system) would lead to significant savings in capital costs. The possible integration of a PTES system with a CSP plant has not yet been proposed and investigated in literature, to the author's knowledge. To demonstrate the benefits led by the integration of solar power plants and PTES systems, a simulation model for the integrated PTES-CSP plant has been developed on MATLAB environment. As case study, an integrated PTES-CSP system using argon as working fluid and with a nominal power of 5 MW and a nominal storage capacity of 4 equivalent hours of operation has been considered. A design approach for determining the operating conditions of the two sections under nominal conditions has been proposed. The influence of the main design parameters on the performance indexes, namely, the roundtrip efficiency of the PTES section and the charge-to-discharge efficiency of the integrated PTES-CSP section, has been investigated with the aim of finding the optimal cycle configuration in terms of compressor pressure ratio and TES operating temperatures. An analysis on the required TES volumes has been also carried out, considering their operating temperatures and the required storage capacity. Moreover, a sensitivity analysis on the compressor and turbine efficiencies and on the circuit pressure drop has been conducted. Finally, the overall performance indexes have been compared with those found by using air as working fluid.

2. System Configuration

A schematic of the integrated PTES-CSP plant investigated in this paper is shown in Fig. 1. The two main sections (PTES and CSP sections) use the same working fluid and share most of the plant components. In particular, the PTES section operates with a closed loop reversed Brayton cycle while the CSP section operates with a closed loop direct Brayton cycle. The aim of the two sections is to store the electricity surplus of the grid and to produce electricity from solar energy, respectively. The energy sources of the two sections are both characterized by fluctuations in their availability, due to the intermittent nature of the solar radiation and the operating conditions of the grid and its requirements of ancillary services. To face this fluctuations and to enhance the flexibility of the overall integrated plant (as designed, the two sections can operate simultaneously or independently from each other), three TES systems are introduced: a high-temperature TES (HT-TES) for dealing with the intermittence in solar energy availability and increasing the capacity factor of the CSP section; a medium temperature TES (MT-TES) and a low temperature TES (LT-TES) for the proper operation of the PTES system. Due to the use of gaseous working fluids, a single tank thermocline packed bed system is used for all the three TES sections. Granite pebbles are chosen as solid storage media for the wide temperature range this material can operate and for its low cost. Moreover, the integrated plant includes the solar field, a low-pressure (LP-C) and a high-pressure compressor (HP-C) as well as a low-pressure (LP-T) and a high-pressure turbine (HP-T).

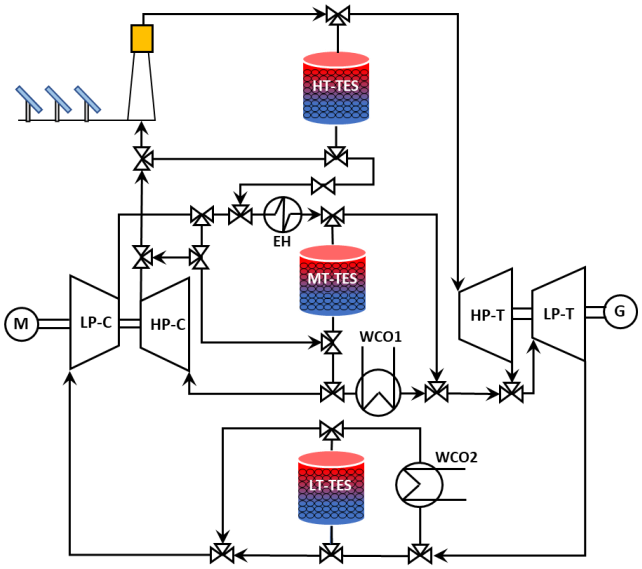

Fig. 1 – System configuration of the integrated PTES-CSP plant.

Furthermore, as shown in the figure, two heat exchangers, an electrical heater and several three-ways and bypass valves are included in the system with the purpose of allowing the different operating modes. Fig. 2 shows the four operating modes of the integrated PTES-CSP plant. In fact, owing to the seasonality of the solar energy availability, the CSP section would operate especially during summer and mid-seasons, with a drop in the operating hours during winter. On the other hand, the operability of the PTES section should be guaranteed throughout the year and independently from solar availability. The charging and discharging phases of the PTES section without the contribution of the CSP plant are labelled mode A and B, respectively. As depicted in the figure, the operation of the PTES section alone requires the use of the low-pressure compressor LP-C, the low-pressure turbine LP-T and of the medium and low temperature TES systems. During the PTES charging phase (mode A), the electricity surplus of the grid is used by the LP-C to pressurize the working fluid with the consequent increase of both pressure and temperature. If required, an electrical heater (EH) can be included to further increase the temperature of the working fluid. As discussed in the following sections, this component is optional, and its introduction is a design choice. The working fluid is cooled in the MT-TES, which increases its state-of-charge, and then in a water cooler (WCO1) until the design turbine inlet temperature is reached. Subsequently, the working fluid expands in the low-pressure turbine down to the minimum pressure of the cycle. Since the turbine outlet temperature is lower than the design compressor inlet temperature, the working fluid is suitably heated up in the LT-TES. Consequently, during the PTES charging phase the net energy absorbed from the grid (that is the difference between the energy required by the compressor and that produced by the turbine) is used to “pump” heat from the LT-TES to the MT-TES. During the PTES discharging phase (mode B), the high temperature energy stored in the MT-TES is used to heat the compressed working fluid before expanding in the turbine. In this case, the EH and WCO1 components are not active while a second water cooler (WCO2) is required to reduce the turbine outlet temperature of the working fluid down to the maximum temperature set for the LT-TES. The thermal energy subtracted by the WCO2 is available for external uses while the working fluid cooling process is completed by the LT-TES. The charging and discharging phases of the PTES integrated with the CSP plant define the operating modes C and D, respectively. In particular, since the PTES charging phase occurs during electrical energy overproduction periods, the delivery of power from the CSP section is not convenient for both the plant owner, since the selling prices are usually low in these conditions, and the Transmission System Operator (TSO), since it would further affect the grid power balance. For this reason, this operating mode is used only to charge all the TES systems. Therefore, unlike the mode A, the compressed working fluid is firstly sent to the solar receiver, where its temperature increases, before feeding the HT-TES. This storage section is arranged to return the working fluid with a temperature equal to that set as the maximum inlet temperature of the MT-TES. Then, the PTES section operates as explained for mode A. It is worth noting that, in this operating mode, no electrical heater is required after the compressor.

Consequently, during the charging phase of mode C, the net energy absorbed from the grid (that is the difference between the energy required by the compressor and that produced by the turbine) is used to “pump” heat from the LT-TES to the HT-TES and MT-TES.

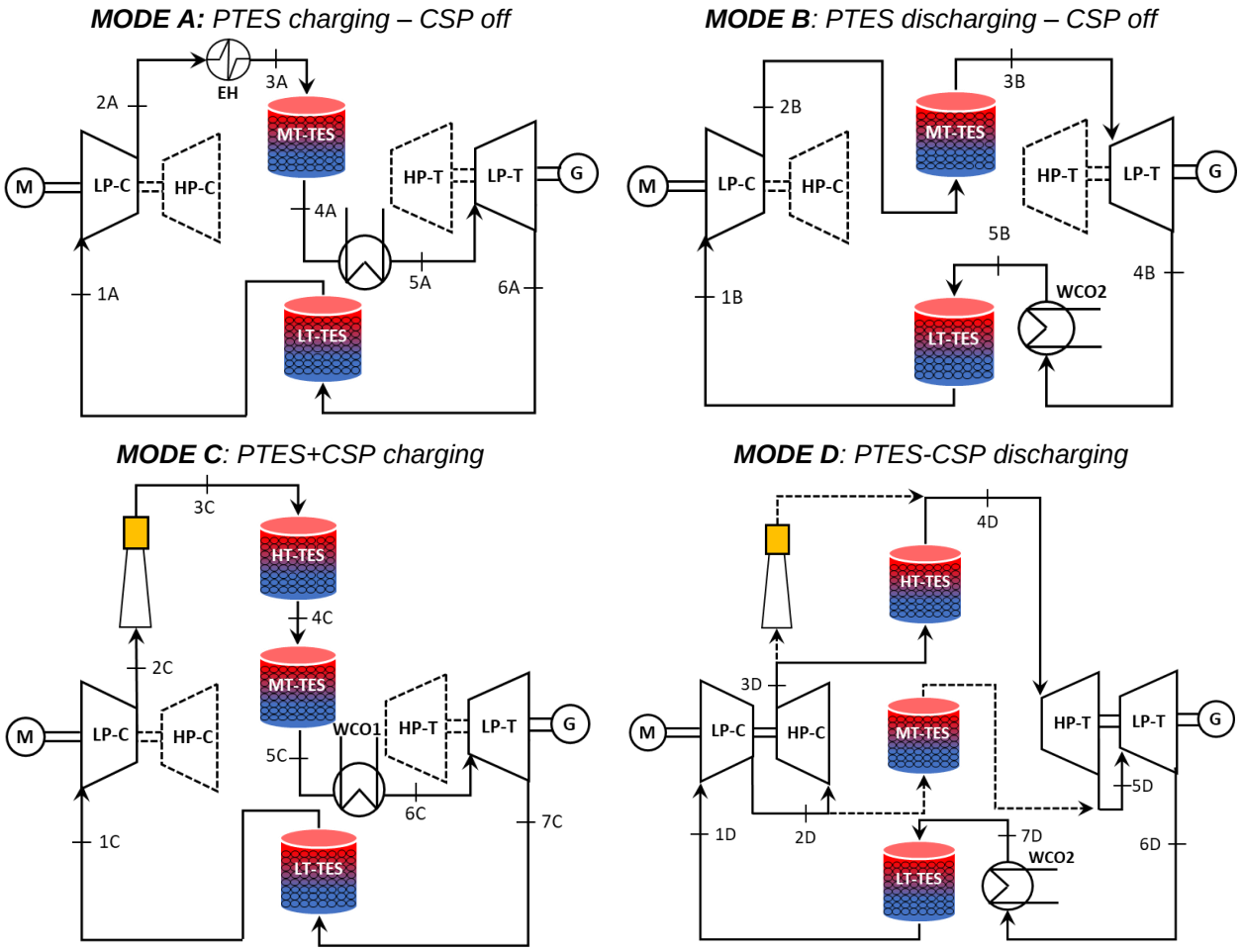

Fig. 2. Schematics of the four operating modes defined for the integrated PTES-CSP plant.

The latter are also charged by using the thermal energy produced by the solar field. During the PTES-CSP discharging phase (mode D), the high temperature energy stored in the HT-TES and MT-TES, together with the energy produced by the solar field, is used to heat the compressed working fluid before expanding in the turbines. The working fluid is heated up to the maximum temperature in the HT-TES system and/or in the solar receiver before a first expansion in the high-pressure turbine. As a design choice, this first expansion is arranged to have a temperature and pressure of the working fluid at the inlet side of the second expander equal to that found in mode B. After this first expansion, the working fluid follows the same path of mode B. During the operating phase, a share of the mass flow could be sent to the MT-TES instead of the CSP section depending on solar availability and state-of-charge of the HT-TES, but this case is not considered.

3. Mathematical model

In this section, the mathematical models developed in MATLAB environment to simulate the main components of the PTES-CSP plant and to calculate the main performance indexes are introduced. Coolprop database [10] is used for the evaluation of working fluid properties.

3.1 Design-stage

During the design-stage of the PTES-CSP plant, the determination of the two thermodynamic cycles and the sizing of the main components is carried out. In detail, in a first step, the operating pressure and temperature under design conditions are defined for a given working fluid. A minimum cycle pressure of 0.5 bar and a LP compressor inlet temperature of 300 K during charging phases (modes A and C) are imposed, while the polytropic efficiency of the turbines and compressors is set to 0.90. Consequently, all the thermodynamic states can be determined by setting three design parameters, namely, the pressure ratio of the low-pressure compressor (β_{LP}), the pressure ratio of the high-pressure compressor (β_{HP}) and the maximum temperature achieved in the solar receiver (T_{MAX}).

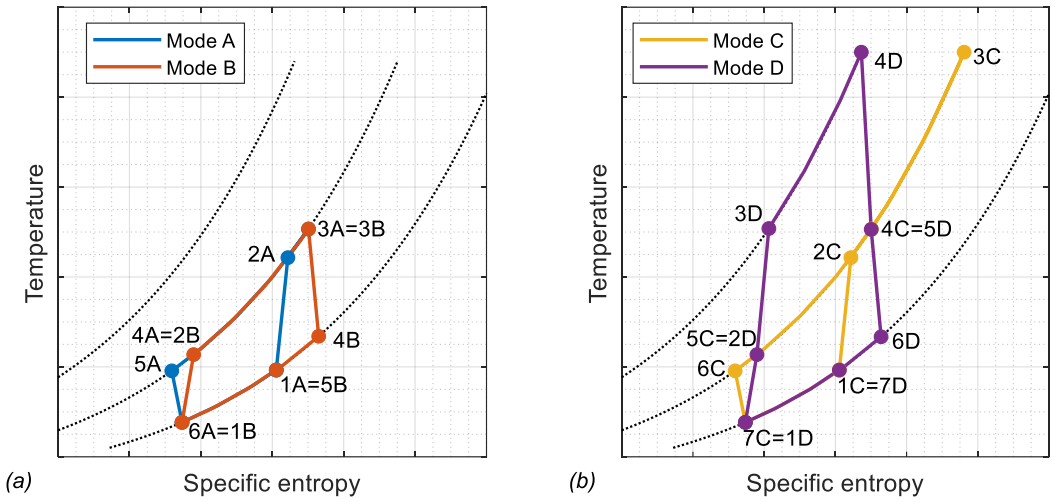

Fig. 3 -Typical thermodynamic cycles followed by the integrated systems in the four operating modes.

Fig. 3 shows an example of the thermodynamic cycles followed in the four operating modes introduced in the previous section. As can be observed, the four thermodynamic cycles are strictly connected and the operating conditions under design conditions should assure constant temperature differences in the three TES sections regardless the operating mode. This link among the two cycles is obtained by means of two constraints: (1) the maximum temperature reached in the MT-TES (and, thus, the LP-T inlet temperature) must be the same independently from the operating mode, which means that the maximum PTES temperature ($T_{3A} = T_{3B}$) must be equal to the HP-T outlet temperature (T_{5D}), and (2) the minimum temperature reached in the HT-TES during charging mode (T_{4C}) must be equal to the HP-C outlet temperature (T_{3D}), which constraints both the minimum LT-TES temperature ($T_{6A} = T_{1B} = T_{7C} = T_{1D}$) and the turbine inlet temperature during the two charging phases ($T_{5A} = T_{6C}$). By introducing these constraints, the design conditions of the PTES cycles are univocal, and they do not change regardless the contribution or not of the CSP section.

The sizing of the main components can be carried out according to two main design parameters: the nominal power of the integrated PTES-CSP plant ($\dot{W}_{NET}$) and the energy storage capacity of the system (Δt_{TES}), expressed in equivalent hours of operation of the plant under nominal conditions.

In particular, the mass flow rate of the working fluid circulating in the integrated plant ($\dot{m}_{WF}$) is calculated according to the useful power produced during the operating mode D, as:

$$\dot{m}_{WF} = \frac{\dot{W}_{NET}}{[(h_{4D} - h_{6D}) - (h_{3D} - h_{1D})]} \quad (1)$$

where h is the specific enthalpy. The compressors are designed according to the power absorbed during the compression phase of operating mode C, while the expanders are designed based on the power produced during the operating mode D. In this preliminary analysis, it is assumed that the same machines are used regardless the operating mode with a constant polytropic efficiency. Moreover, the study focuses on the cycle assessment and therefore, mechanical losses, auxiliary consumption and solar field efficiency is neglected.

3.2 TES model

As previously reported, the plant requires TES systems at three different temperature levels. Each TES has to be sized to provide the required storage capacity Δt_{TES}. The stored energy (E_{TES}) is calculated as:

$$E_{TES} = \dot{m}_{WF} \bar{c}_{WF} \left(T_{WF,max} - T_{WF.min}\right) \cdot \Delta t_{TES} \quad (2)$$

where $\bar{c}_{WF}$ is the average specific heat, while $T_{WF,max}$ and $T_{WF.min}$ are the maximum and the minimum fluid temperatures inside each TES system, respectively. Starting from the energy stored, the theoretical tank volume ($V_{TES,t}$), namely, the storage volume required if the entire packed bed is heated up from the minimum temperature ($T_{WF,min}$) to the maximum temperature ($T_{WF,max}$), is calculated as follows:

$$V_{TES,t} = \frac{E_{TES}}{(\bar{\rho}_S \bar{c}_S (1-\varepsilon) + \bar{\rho}_{WF} \bar{c}_{WF} \varepsilon) \cdot (T_{WF,max} - T_{WF.min})} \quad (3)$$

where $\bar{\rho}_S$ and $\bar{\rho}_{WF}$ are the average densities of the solid media and working fluid respectively, $\bar{c}_S$ is the specific heat of the solid media and ε is the porosity of the bed, here assumed equal to 0.4. The tank is filled by granite pebbles ($\bar{\rho}_S$ = 2688 kg/m^3), assuring a good compromise between cost, availability and exploitability for a wide temperature range. The main thermal properties are temperature-dependent, according to the correlations obtained from experimental tests [11] [12]. Since a thermocline must be kept inside the bed, it is not possible to exploit completely the TES storage capacity. Consequently, for a given storage capacity, a greater tank volume must be provided, and numerical simulations are required to calculate the temperature profiles over time along the axis of the bed. The latter are determined by simulating the thermal behavior of the TES system with a transient 1-D two-equation model that returns the temperature profiles along the bed for both the working fluid (T_{WF}) and the solid media (T_S) (a constant radial temperature profile was assumed as the bed was considered homogeneous and isotropic) [13]:

$$\varepsilon \rho_{WF} c_{WF} \frac{\partial T_{WF}}{\partial t} + \rho_{WF} c_{WF} u \frac{\partial T_{WF}}{\partial z} = \alpha A_S (T_S - T_{WF}) - U_{TES} A_{TES} (\overline{T}_{WF} - T_{AMB}) \quad (4)$$

$$(1-\varepsilon) \rho_S c_S \frac{\partial T_S}{\partial t} = k_{eff} \frac{\partial T_S}{\partial z^2} + \alpha A_S (T_{WF} - T_{BED}) \quad (5)$$

where k_{eff} is the effective thermal conductivity that takes into account also the radiation contribute [14] within the bed. A_S and α are the superficial area per unit of volume of the bed and the convective heat transfer coefficient, calculated according to previous studies [15], U_{TES} is the overall heat transfer coefficient between tank and environment (set equal to 0.3 W/m^{2}K), A_{TES} is the superficial area per unit of volume of the vessel and T_{AMB} is the ambient temperature.

3.3 Performance indexes

Different indexes are defined and investigated to analyse the integrated PTES-CSP plant performances by varying the main design parameters, such as the two pressure ratios and the maximum temperature. All the performance indexes refer to nominal conditions, with a constant mass flow rate of the working fluid regardless the operating mode. Consequently, the power ratios correspond to the ratios between specific works. The cycle efficiency of the integrated PTES-CSP system during mode D (η_D) is the first performance index. Since during mode C the solar section is only used to charge the HT-TES section without any electrical power production, this index is defined as the ratio between the net power produced during the operating mode D ($\dot{W}_D$) and the thermal power introduced through the solar receiver ($\dot{Q}_S$):

$$\eta_D = \frac{\dot{W}_D}{\dot{Q}_S} = \frac{(h_{4D} - h_{6D}) - (h_{3D} - h_{1D})}{(h_{4D} - h_{3D})} \quad (6)$$

A second performance index is the charge-to-discharge efficiency of the integrated PTES-CSP section ($\eta_{C \to D}$). Since it is assumed that during mode D the system is completely fed by the TES system, this efficiency is the ratio between the power delivered during mode D and the sum of the electrical power ($\dot{W}_C$) and thermal power absorbed during mode C to charge the three TES tanks:

$$\eta_{C \to D} = \frac{\dot{W}_D}{-\dot{W}_C + \dot{Q}_S} = \frac{(h_{4D} - h_{6D}) - (h_{3D} - h_{1D})}{(h_{2C} - h_{1C}) - (h_{6C} - h_{7C}) + (h_{3C} - h_{2C})} \quad (7)$$

This index can be considered as a roundtrip efficiency of the integrated system, but it cannot be compared with roundtrip efficiencies of other storage technologies since it includes a thermal input ($\dot{Q}_S$) that affects in terms of energy amount and quality the energy flows during the charging phase. A third performance index concerns the charge-to-discharge efficiency ($\eta_{A \to B}$) of the only PTES section (corresponding to the PTES roundtrip efficiency), which is defined as the ratio between the electric power produced by the PTES section during the discharging phase (mode B) and the electric power absorbed during charging phase (mode A):

$$\eta_{A \to B} = \frac{\dot{W}_B}{-\dot{W}_A} = \frac{(h_{3B} - h_{4B}) - (h_{2B} - h_{1B})}{(h_{2A} - h_{1A}) - (h_{5A} - h_{6A}) + (h_{3A} - h_{2A})} \quad (8)$$

where the term $(h_{3A} - h_{2A})$ refers to the power absorbed by the electrical heater, if present. Finally, a PTES-to-CSP power ratio (γ) is introduced to investigate the weight of the PTES section compared to the CSP section. This ratio is defined as the ratio between the power produced by the PTES section ($\dot{W}_{PTES,D}$) and the power produced by the CSP section ($\dot{W}_{CSP,D}$) during discharging phase (mode D):

$$\gamma = \frac{\dot{W}_{PTES,D}}{\dot{W}_{CSP,D}} = \frac{(h_{5D} - h_{6D}) - (h_{2D} - h_{1D})}{(h_{4D} - h_{5D}) - (h_{3D} - h_{2D})} \tag{9}$$

4. Results and discussion

In this section, the performance of the integrated PTES-CSP system under design conditions as a function of the different design parameters are presented and discussed. Argon is chosen as working fluid, according to [5,7], while pressure drops are assumed negligible. Fig. 4 shows the performance indexes defined in the previous section as a function of the pressure ratio of both the LP and the HP compressor, by assuming a maximum temperature at the outlet of the solar receiver equal to 1000 K. Fig. 4(a) shows the cycle efficiency obtained during the operating mode D. As expected for a Brayton-Joule cycle, a rise in the performance occurs with the increase of both β_{LP} and β_{HP} and, thus, with the increase of the overall pressure ratio, although the benefits become more and more marginal with their increase. The index η_D ranges between 0.30 and 0.70, values rather high due to the very low LP-C inlet temperature (below 200 K) thanks to the presence of the LT-TES, which was charged during the operating mode C. Therefore, this performance index gives important information about the conversion efficiency achievable by the integrated plant but does not consider the performance of the system during the charging phase of the various TES tanks. Subsequently, the charge-to-discharge efficiency of the integrated PTES-CSP plant, shown in Fig. 4(b), is more explanatory of the effective performance obtained by the plant. As depicted in this figure, the benefits in increasing β_{HP} are reflected also on this performance index, while the effect of the LP-C pressure ratio on the $\eta_{C\to D}$ is not significant. In fact, the benefits arising from the increase of the pressure ratio during the discharging phase (mode D) are counteracted by a performance degradation during charging phase (mode C), due to the increased weight of the irreversibility in the turbomachines with the rise of β_{LP}. Fig. 4(c) shows the charge-to-discharge efficiency of the PTES section without solar contribution ($\eta_{A\to B}$). This performance index ranges between 0.10 and 0.62, increases with β_{HP} and reaches its maximum for a given value of β_{LP}.

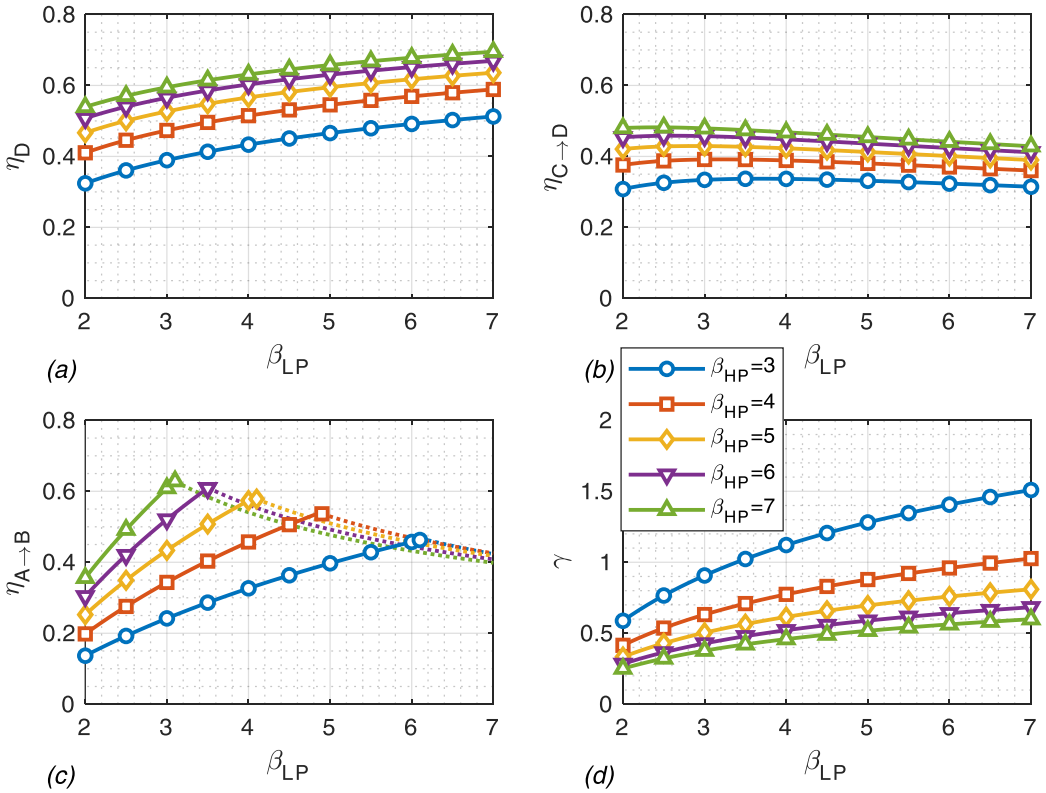

Fig. 4 – Main performance indexes achieved by the integrated PTES-CSP plant as a function of the two pressure ratios by assuming a maximum temperature of 1000 K.

This behaviour is due to the temperature difference between the MT-TES inlet side and the LP-C outlet side ($(T_{3A} - T_{2A})$ in Fig. 3). As mentioned, an electrical heater is used to increase the working fluid temperature up to the required maximum temperature. However, this temperature difference and, thus, the contribution of the electrical heater decreases with β_{LP}, up to the maximum PTES roundtrip efficiency, where $T_{3A} = T_{2A}$ and no electrical heating is required. A further increase of β_{LP} would result in a negative temperature difference, with the corresponding requirement of a cooling system after the LP compressor (this operating condition was not considered in this study). The value of β_{LP} in which the maximum of the $\eta_{A\to B}$ is achieved depends on both β_{HP} and T_{MAX}. For a given value of T_{MAX}, the temperature T_{3A} decreases with the rise in the HP-C pressure ratio due to the two constraints introduced for the two thermodynamic cycles, and higher values of β_{LP} are required to avoid the use of an electrical heater.

On overall, the effect of the two pressure ratios is not univocal. The use of high β_{HP} is beneficial for both the charge-to-discharge efficiencies analysed, but its benefits becomes more and more marginal with its rising. Moreover, as shown in Fig. 4(d), the PTES-to-CSP power ratio could reach too low values and the corresponding maximum pressure could be problematic for the design of the solar receiver and the HT-TES. The trend obtained for $\eta_{A\to B}$ suggests to operate with high values of β_{LP}, leading also to an increase of the PTES-to-CSP power ratio (see Fig. 4(d)), even if negative temperature differences between the MT-TES inlet side and the LP-C outlet side may occur. The best compromise could be achieved by assuming no electrical heater during design conditions: in this case the imposed β_{LP} depends on β_{HP} and T_{MAX}. A further element of investigation concerns the operating conditions of the three TES systems. Fig. 5 shows the main temperatures at the inlet/outlet of the three storage devices together with the mass flow rate circulating in the power block. Fig. 5(a) shows the LP-T exit temperature (T_{6A}), that is the LT-TES inlet temperature during the discharging phase of the PTES section. T_{6A} is the minimum cycle temperature and varies in the range 100-300 K, with the lowest values obtained for high pressure ratios just above the boiling point of liquid argon for the assumed minimum pressure (0.5 bar). Consequently, the storage of this cryogenic energy could be a challenging task and could introduce a strong limitation in the choice of the design parameters. As shown by Fig. 5(b-c), the effect of β_{LP} on the LP-T inlet temperatures during the charging and discharging phases, namely, T_{5A} and T_{3A} respectively, is minor (T_{5A}) or negligible (T_{3A}), while these temperatures decrease with β_{HP}. The WCO1 exit temperature (T_{5A}) is below 290 K for β_{HP} higher than 4. This would require an uncommon cooling system based on chillers with the subsequent increase of capital and operating costs.

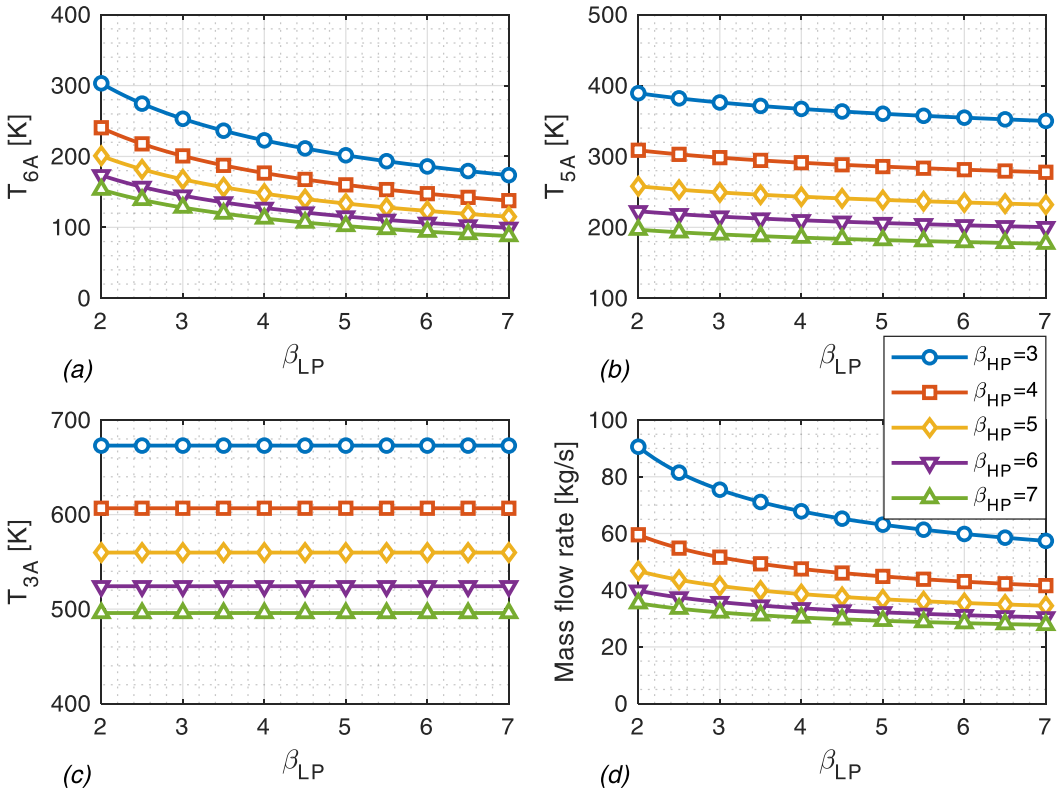

Fig. 5 – Minimum temperatures required in the (a) LT-TES, (b) MT-TES and (c) HT-TES and (d) mass flow rate circulating in the power block.

It is worth noting that the temperature difference required in the MT-TES (that is T_{3A}-T_{4A}) remains almost constant (about 300 K) with the variation in the pressure ratios. Since T_{3A} corresponds also to the minimum temperature of the HT-TES, the increase of the HP-C pressure ratio also increases the temperature differences at the HT-TES (the maximum temperature is constant), which ranges between 350K and 500 K. Fig. 5(d) shows that, as expected, the increase of the two pressure ratios lead to lower working fluid mass flow rates. Fig. 6 shows the effect of the maximum cycle temperature (set equal to 1000 K in the previous analysis) and the LP compressor inlet temperature (previously set equal to 300 K), on the main performance indexes. Fig. 6 refers to a β_{HP} equal to 4 to avoid an outlet temperature at the water cooler (WCO1) lower than the ambient one and to a β_{LP} suitable to avoid the presence of the electrical heater during mode A. As shown in Fig. 6 (a) and (b), the main performance indexes remain almost constant with the variation of the two input temperatures, due to the marginal variation of the specific heat with temperature of the working fluid. On the other hand, γ is strongly influenced by the two design temperatures. As shown in Fig. 6 (c), a rise in T_{MAX} results in an increase of γ while an increase in the T_{1A} strongly reduces both the LP compressor pressure ratio and, consequently γ. Therefore, to obtain a constant PTES-to-CSP power ratio, the increase of 25 K in the T_{1A} requires the simultaneous increase of about 80 K in the T_{MAX}. Finally, the advantages in increasing the T_{1A} are shown in Fig. 6 (d): for a given rise in the T_{1A}, a rise in the WCO1 exit temperature is observed, allowing the use of water as cooling fluid. An increase of the minimum temperature of the LT-TES (T_{5A}) also occurs, reducing the potential issue concerning the storage of cryogenic energy.

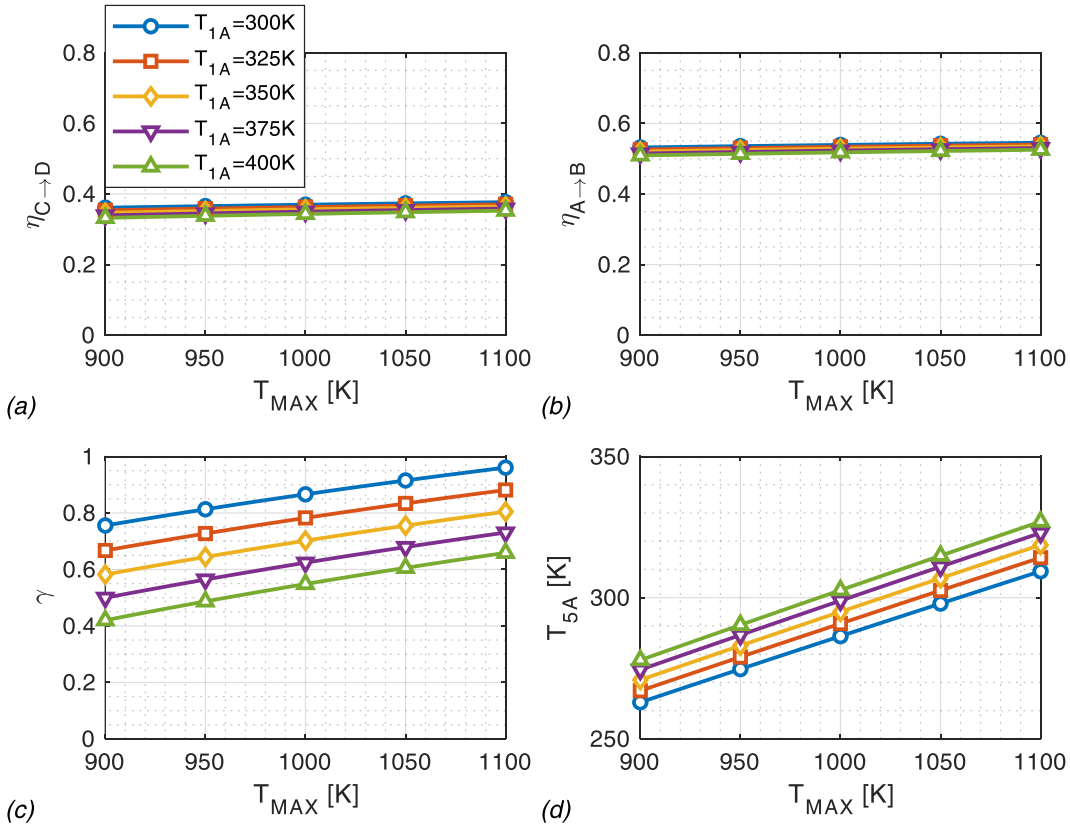

Fig. 6 - Main performance indexes achieved by the integrated PTES-CSP plant as a function of maximum cycle temperature and LP compressor inlet temperature.

4.1 TES design

As demonstrated by the previous analysis, the choice of the main design parameters should be the best compromise between the maximization of the performance indexes and the minimization of technical issues. In particular, the latter are mainly related to the minimum and maximum temperatures reached by storage materials, tank insulation losses and operating pressures of both solar receiver and HT-TES. A preliminary design of the integrated PTES-CSP plant is reported in Table 1, while Table 2 reports the storage volume required for the three storage tanks, in terms of theoretical ($V_{TES,t}$) and actual vessel volume ($V_{TES,r}$) and the corresponding diameter and height (an aspect ratio of 3 was assumed). Although the difference between the

maximum and minimum temperature of the working fluid along the bed varies with the three storage systems considered, the required volume is almost the same. As shown in Fig. 7(a), the specific heat of the granite pebbles strongly increases with temperature, with a corresponding decrease of the storage volume. As already mentioned, the need of keeping fixed temperatures at the inlet and outlet side of the packed bed results from the presence of a thermocline inside the tank at the end of each cycle. By way of example, Fig. 7(b) shows the temperature profile of the MT-TES obtained after a fully charging and a fully discharging phase, highlighting the useful storage zone as the area enclosed between the two temperature profiles (possible hysteresis effects are not considered in this study).
Consequently, as reported in Table 2 the actual storage volume required by the three TES systems is about three times the minimum storage volume, although a tolerance in outlet temperature of 20 K is imposed.

Table 1 – Preliminary design of the integrated PTES-CSP plant.

Design parameters		**Performance**	
LP compressor pressure ratio (β_{LP})	3.5	PTES-CSP cycle efficiency (η_D)	49.6%
HP compressor pressure ratio (β_{HP})	4	PTES-CSP charge-to-discharge eff. ($\eta_{C\to D}$)	35.7%
Maximum Temperature (T_{MAX})	1000 K	PTES charge-to-discharge efficiency ($\eta_{A\to B}$)	52.3%
LP compressor inlet temperature (T_{1A})	350 K	PTES-to-CSP power ratio (γ)	0.700
LP compressor inlet pressure (p_{1A})	0.5 bar	PTES nominal power	2.05 MW
Working fluid	Argon	CSP nominal power	2.95 MW

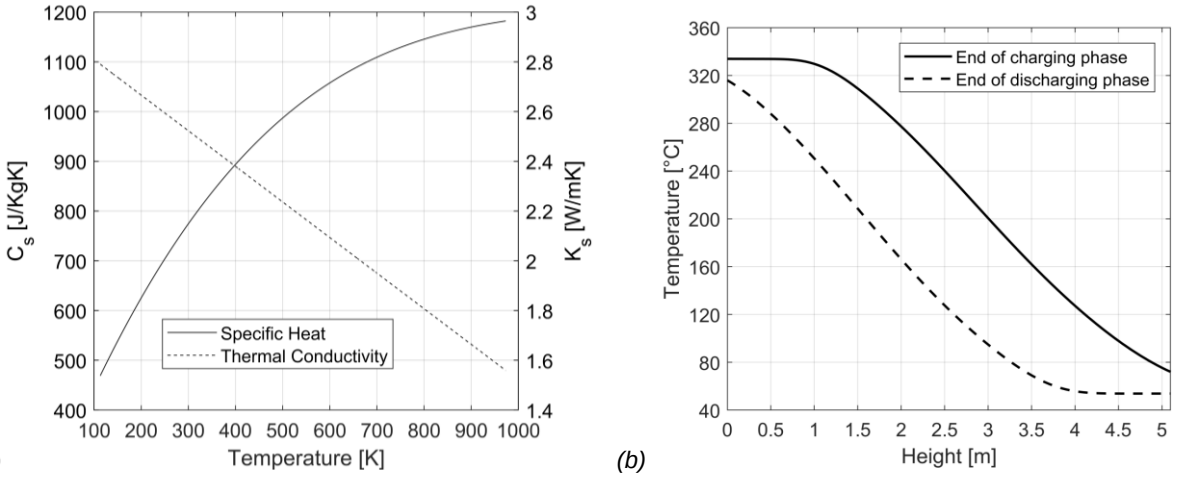

(a) *(b)*

Fig. 7: (a) Specific heat and thermal conductivity of the granite pebbles over temperature and (b) temperature profiles of the MT-TES at the end of the charging and discharging phases.

Table 2 – Main design parameters for the three TES systems of the proposed PTES-CSP plant.

Storage system	**ΔT [K]**	$V_{TES,t}$ **[m³]**	$V_{TES,r}$ **[m³]**	**Diameter [m]**	**Height [m]**
LT-TES	162	330	884	15.0	5.0
MT-TES	280	254	938	15.3	5.1
HT-TES	392	211	832	14.7	4.9

4.2 Influence of turbomachinery efficiencies and pressure losses

A sensitivity analysis has been carried out to investigate the effect on the two charge-to-discharge efficiencies of two important parameters, namely, the polytropic efficiency of compressors and expanders and the circuit pressure drops. Fig. 8 shows the variation of the main performance indexes with the polytropic efficiency (since this parameter is explanatory of the technology level of the turbomachines, no difference among compressors and expanders is introduced) for different values of relative pressure drops in given components (it is assumed that pressure drops are concentrated in the three TES systems and in the solar receiver). As shown in Fig. 8(b), the turbomachines efficiency strongly influences the PTES roundtrip efficiency. This fact, already demonstrated by other published papers [5,7], highlights the need of compressors and expanders with a high technology level if competitive roundtrip efficiencies wants to be achieved. Moreover, the design of the TES systems in terms of aspect ratio, bed void fraction, average

pebble diameter should be optimized by considering the thermal performance of the TES, but also the pressure drops introduced in the circuit. As shown in Fig. 8(a), the charge-to-discharge efficiency is less sensitive to pressure losses if the plant operates in integrated mode, although a decrease of 5 percentage points is observed by assuming relative pressure losses of 10% in the main plant component compared to the case with negligible pressure losses.

4.3 Use of air as working fluid

The comparison in the use of air instead of argon as working fluid is shown in Fig. 9, by assuming a maximum temperature of 1000 K and a LP-C inlet temperature during charging phases (modes A and C) of 300 K. In particular, Fig. 9(a) shows the variation of the charge-to-discharge efficiencies with and without the CSP contribution as a function of the PTES-to-CSP power ratio. As can be observed, slightly variations in the performance indexes are achieved by using air instead of argon, with a minor increase in the $\eta_{C\to D}$, but a simultaneous slight decrease in the $\eta_{A\to B}$. However, the use of air leads to higher values of γ, which means that the nominal power of the PTES section is equal or even higher than the CSP plant one, even if the use of air leads to lower efficiencies. Moreover, values of γ higher than 0.75 are not achievable with Argon since the minimum temperature in the LT-TES reaches its liquefaction temperature. On the other hand, the minimum values of γ reached by using air are higher than 0.25, instead of values around 0.1 achieved by using Argon, which are also characterized by the maximum performance indexes. Another important difference concerns the pressure ratios required to obtain given values of γ. As shown by Fig. 9(b), higher pressure ratios are required by air to reach a given PTES-to-CSP power ratio. This can be a challenging issue for the design of both solar receiver and HT-TES system, which would operate with pressures higher than 50 bar. The higher specific heat of air results in a decrease of the temperature differences required in the TES systems, with a consequent increase of the minimum temperature observed in the MT and LT-TES and, at the same time, the possibility of operating with higher β_{LP} and, thus, achieving higher γ.

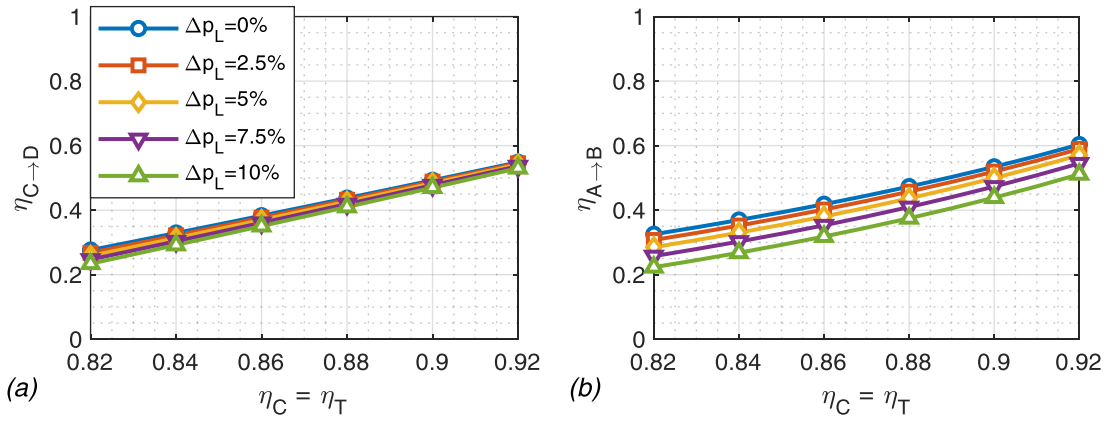

Fig. 8 -Effect of compressor and turbine polytropic efficiency and TES pressure losses on the charge-to-discharge efficiencies.

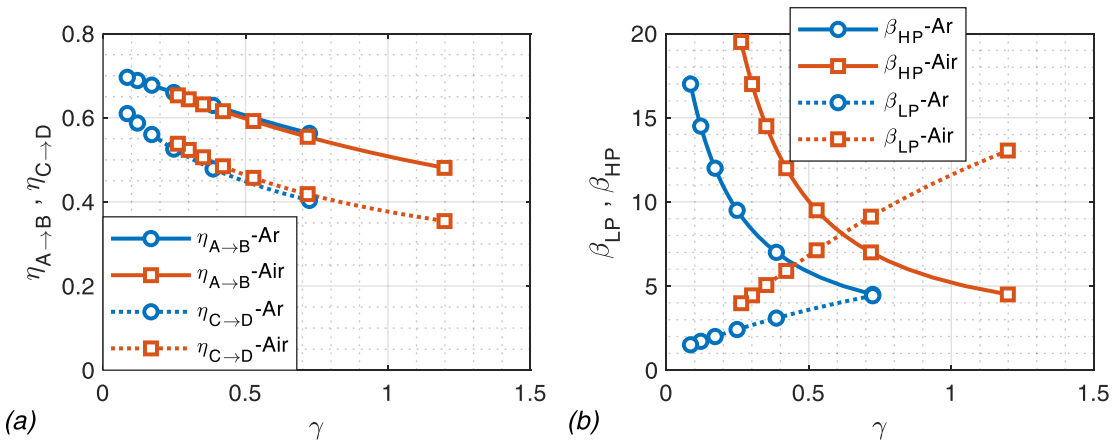

Fig. 9 – Comparison in the achieved performance indexes and required pressure ratio in function of PTES-to-CSP power ratio by using air or argon as working fluid.

5. Conclusions

An innovative PTES system integrated with a CSP plant based on a closed loop Brayton-Joule cycle was proposed and analysed in this study. The integrated PTES-CSP system uses argon as working fluid and includes three different TES systems. Specific mathematical models were developed to simulate the PTES and CSP sections as well as to calculate the thermal behaviour of the different TES storage tanks during the charging and discharging processes and to assess the required storage volumes. The study demonstrates that the operating parameters and the constraints introduced to connect the two main sections strongly influence the integrated plant performance and in particular the charge-to-discharge efficiencies. On overall, the use of high-pressure ratios is beneficial for the charge-to-discharge efficiencies, even if the benefits become more and more marginal with the rise of the pressure ratio. Moreover, too high operating pressures could be detrimental for the design of the solar receiver and the high temperature storage tank. The inclusion of an electrical heater after the LP compressor improves the flexibility of the integrated system, but, as expected, it results detrimental from an energetic point of view. The low temperature TES operates under cryogenic conditions, but an increase in the minimum temperature can be achieved by increasing the inlet temperature of the LP compressor. A feasible design of the PTES-CSP system with a rated power of 5 MW and 4 hours of storage capacity was then proposed, achieving a PTES-CSP charge-to discharge efficiency of about 36%. On the other hand, since all the plant components should frequently operate far from their nominal conditions (due to fluctuation on both storage service requirements and solar energy availability), the actual capabilities of the integrated system should be investigated during operating conditions. For this reason, the development of specific mathematical models for investigating the plant performance under off-design conditions, as well as the study of suitable control strategies for the optimum management of the integrated plant, are currently under development for future works.

References

[1] G.F. Frate, L. Ferrari, U. Desideri, Multi-criteria investigation of a pumped thermal electricity storage (PTES) system with thermal integration and sensible heat storage, Energy Convers. Manag. 208 (2020) 112530. doi:10.1016/j.enconman.2020.112530.

[2] A. White, G. Parks, C.N. Markides, Thermodynamic analysis of pumped thermal electricity storage, Appl. Therm. Eng. 53 (2013) 291–298. doi:10.1016/j.applthermaleng.2012.03.030.

[3] A. Benato, A. Stoppato, Pumped Thermal Electricity Storage: A technology overview, Therm. Sci. Eng. Prog. 6 (2018) 301–315. doi:10.1016/j.tsep.2018.01.017.

[4] J. Guo, L. Cai, J. Chen, Y. Zhou, Performance evaluation and parametric choice criteria of a Brayton pumped thermal electricity storage system, Energy. 113 (2016) 693–701. doi:10.1016/j.energy.2016.07.080.

[5] J.D. McTigue, A.J. White, C.N. Markides, Parametric studies and optimisation of pumped thermal electricity storage, Appl. Energy. 137 (2015) 800–811. doi:10.1016/j.apenergy.2014.08.039.

[6] A. Benato, Performance and cost evaluation of an innovative Pumped Thermal Electricity Storage power system, Energy. 138 (2017) 419–436. doi:10.1016/j.energy.2017.07.066.

[7] L. Wang, X. Lin, L. Chai, L. Peng, D. Yu, H. Chen, Cyclic transient behavior of the Joule–Brayton based pumped heat electricity storage: Modeling and analysis, Renew. Sustain. Energy Rev. 111 (2019) 523–534. doi:10.1016/j.rser.2019.03.056.

[8] A. Benato, A. Stoppato, Heat transfer fluid and material selection for an innovative Pumped Thermal Electricity Storage system, Energy. 147 (2018) 155–168. doi:10.1016/j.energy.2018.01.045.

[9] O. Dumont, G.F. Frate, A. Pillai, S. Lecompte, M. De paepe, V. Lemort, Carnot battery technology: A state-of-the-art review, J. Energy Storage. 32 (2020) 101756. doi:10.1016/j.est.2020.101756.

[10] I.H. Bell, J. Wronski, S. Quoilin, V. Lemort, Pure and Pseudo-pure Fluid Thermophysical Property Evaluation and the Open-Source Thermophysical Property Library CoolProp, Ind. Eng. Chem. Res. 53 (2014) 2498–2508. doi:10.1021/ie4033999.

[11] L. Chai, J. Liu, L. Wang, L. Yue, L. Yang, Y. Sheng, H. Chen, C. Tan, Cryogenic energy storage characteristics of a packed bed at different pressures, Appl. Therm. Eng. 63 (2014) 439–446. doi:10.1016/j.applthermaleng.2013.11.030.

[12] L. Livermore, High-temperature Mechanical , Physical ° I, 20 (1983) 3–10.

[13] G. Zanganeh, A. Pedretti, S. Zavattoni, M. Barbato, A. Steinfeld, Packed-bed thermal storage for concentrated solar power - Pilot-scale demonstration and industrial-scale design, Sol. Energy. 86 (2012) 3084–3098. doi:10.1016/j.solener.2012.07.019.

[14] J.M.S. D. Kunii, Heat transfer characteristics of porous rocks, A.I.Ch.E. J. 6. (1960) 71–78.

[15] M. Cascetta, F. Serra, S. Arena, E. Casti, G. Cau, P. Puddu, Experimental and numerical research activity on a packed bed TES system, Energies. 9 (2016). doi:10.3390/en9090758.